ISSN 0010-9525, Cosmic Research, 2023, Vol. 61, Suppl. 1, pp. S80–S88. © Pleiades Publishing, Ltd., 2023.
Russian Text © The Author(s), 2022, published in Sovremennyie Problemy Distantsionnogo Zondirovaniya Zemli iz Kosmosa, 2022, Vol. 19, No. 6, pp. 222–233.

Analysis of Hydrological Changes in Mineral Lakes in Northern Eurasia Based on *SMOS* Satellite Data

A. N. Romanov[a], *, I. V. Khvostov[a], **, I. V. Ryabinin[a], *, and D. A. Romanov[a]**

[a] *Institute of Water and Environmental Problems, Siberian Branch, Russian Academy of Sciences, Barnaul, 656038 Russia*

**e-mail: romanov_alt@mail.ru*

***e-mail: nii@mail.ru*

****e-mail: cgsienna@gmail.com*

accepted December 2, 2022

Abstract—The climatic changes taking place in Northern Eurasia, which have become especially aggravated in the past few decades, in combination with the anthropogenic impact on ecosystems, are causing noticeable changes in the hydrological characteristics of mineral lakes. Based on the results of daily measurements of brightness temperature T_b from the *SMOS* (Soil Moisture and Ocean Solution) satellite, the long-term seasonal dynamics of hydrological changes in some large mineral lakes of Northern Eurasia (Caspian Sea, Kara-Bogaz-Gol Bay, Aral Sea, lakes Sarykamyshskoe, Kulunda, Ubsu-Nur) from 2012 to 2022 was studied. The analysis of the seasonal and interannual dynamics of T_b and thermodynamic temperature of the underlying surface was performed on the basis of the *SMOS* L1C and *MODIS* MOD11A1 (Moderate Resolution Imaging Spectroradiometer) products, respectively. Four periods were identified with different behavior of the radiative characteristics of mineral lakes, associated with a decrease in temperature below the freezing point of salt water, the formation and melting of ice cover on the water surface, changes in the area of the water table, and salinity of water. In the northern Caspian Sea, the influence of the phenological phases of ice cover on the change in the microwave radiation of the underlying surface was noted. The features of microwave radiation of the western (deep water) and northern parts of the Aral Sea are studied. The seasonal dynamics of T_b is associated with the processes of formation of ice cover on the water surface. Judging by the changed seasonal dynamics of the T_b, the Sarykamysh Lake was transformed into a year-round ice-free lake. Peculiarities of the seasonal dynamics of T_b for Lake Ubsu-Nur are revealed that may be associated with rainfall in the winter–spring season, as well as with the early opening of rivers and flooding of the ice cover of the lake with river water.

Keywords: salt lakes of Northern Eurasia, remote sensing, microwave range, radio brightness temperature, *SMOS* satellite

DOI: 10.1134/S0010952523700648

INTRODUCTION

Mineral lakes, which are widespread across the globe and found in different regions of the world, are extremely sensitive to climate change. Water level and water-surface area are specific indicators of climate change are [36]. During low-water periods, lakes of small area may dry out partially or completely [14, 33]. The drying out of large lakes affects many atmospheric and hydrosphere processes occurring on a regional and global scale. The atmospheric transfer of toxic salts from the surface of the water and the dried bottom of the lake contributes to an increase in soil salinity, which, in turn, leads to suppression of vegetation cover, changes in the species composition of vegetation and desertification [13].

Current information on hydrological changes in large mineral lakes, which is of great importance in planning measures to protect the environment and adapt society to new living conditions, can be obtained based on space monitoring methods [18, 28]. An important task is to study the long-term seasonal dynamics of radio brightness temperature T_b(JD) (Julian Day) of the underlying surface in different regions of Northern Eurasia, depending on meteorological conditions, as well as on the area and radio emission characteristics of different landscapes (water surface, exposed bottom dry lake, soil cover, forest) [17].

The microwave radiation of the underlying surface, which includes a mineral lake, can vary within significant limits. For example, T_b of a drying salt Lake Eyre (Australia), determined from the *SMOS* (Soil Moisture and Ocean Solution) satellite data, changes during the season from T_b of water surface temperature to T_b of dry soil temperature [21]. Using satellite data from *ALOS PALSAR* (Advanced Land Observing Satellite; Phased Array type L-band Synthetic Aperture Radar), the coastline of the dried-up Lake Lop Nur, located in the eastern part of the Tarim Basin in north-

Fig. 1. Schematic map of the location of test sites in Northern Eurasia. (*1*, *2*) Northern and southern parts of the Caspian Sea, (*3*) Kara-Bogaz-Gol Bay; (*4*) Lake Sarykamysh; (*5*, *6*) western and northern parts of the Aral Sea; (*7*) Lake Kulunda; (*8*) Lake Ubsu-Nur.

western China, was contoured [24]. For remote monitoring of the drying out of mineral lakes, data from *EOS/MODIS* (MOD13Q1) (Earth Observing System/Moderate Resolution Imaging Spectroradiometer) [34], as well as *Landsat-5 TM* and *Landsat-8* [10], are used. The paper [19] studied seasonal variations in T_b of mineral lakes, the area of which is smaller than the area of the *SMOS* pixel. It has been shown that seasonal variations in T_b depend on physical temperature and water salinity, as well as the presence and thickness of ice cover formed on the water surface during the cold period.

MATERIALS AND METHODS

The main objects of the study were large mineral lakes of Northern Eurasia, differing in water surface area, water salinity, concentration and type of dissolved salts, located in different natural zones, at different altitudes above sea level (northern and southern parts of the Caspian Sea, Kara-Bogaz-Gol Bay, sections of the Aral Sea after catastrophic drying out, and Sarykamysh, Kulunda, and Ubsu-Nur lakes) (Fig. 1).

The microwave radiation of the underlying surface, recorded by the sensors of the 2D MIRAS (Microwave Imaging Radiometer with Aperture Synthesis) radiometer (1.41 GHz) and calibrated in units of radio brightness temperature T_b, was extracted from SMOS products [35] of the L1C processing level version v620 [12]. This study presents T_b values measured at horizontal polarization at a probing angle of 42.5°. The longitudinal and transverse spatial resolution of the radiometer is 64 and 35 km, respectively. L1C data are georeferenced to the discrete geodetic grid DGG ISEA 4H9 (Discrete Global Grid Snyder Icosahedron grid with equal area) [23]. The linear size of the cells of this grid is 16 km, the area is 195 km^2. The T_b value for any cell in the L1C product is determined by a section of the Earth's surface with an area of 1760 km^2.

For a homogeneous, slightly rough underlying surface, T_b can be calculated using the formula [15, 25, 32]

$$T_b = \chi T,$$

where χ and T are the emissivity and physical temperature of the underlying surface.

When areas with different radio-emitting characteristics (lakes, coastal zones, and adjacent land areas with poorly developed vegetation) fall into the geodetic grid, the measured T_b values represent a superposition T_b^j of these areas, taking into account the contribution of their areas to the total area of the emitting surface area [20]. In this case, T_b can be calculated using the formula

$$T_b = \sum_{j=1}^{n} T_b^j S_j,$$

where T_b^j and S_j are the radio brightness temperature and area of individual areas.

Respectively, T_b^i of a separate ith section with area S_i at known values of T_b^j and S_j for other areas can be calculated using the formula

$$T_b^i = \frac{\left(T_b - \sum_{\substack{j=1 \\ j\neq i}}^{n} T_b^j S_j\right)}{S_i}. \quad (1)$$

RESEARCH RESULTS

Figure 2 shows graphs of the long-term seasonal dynamics of T_b(JD) of test sites from 2012 to 2022. The abscissa axis shows the values of the Julian day JD_{2012}, counted from the beginning of the observation period (January 1, 2012). In all graphs, straight lines indicate long-term dependences of T_b and T, which make it possible to assess the changes occurring over the period from 2012 to 2021.

T_b(JD) variations in the northern part of the Caspian Sea (see Fig. 2a) are associated with the seasonal formation of ice cover on the water surface, with changes in ice cover, temperature and salinity of the sea surface [2, 3]. T_b values vary from 90 K during periods of open water to 270 K during periods of freezing. The type of T_b(JD) dependence is typical for reservoirs with seasonal ice cover that forms on the water surface. Numbers 1–4 indicate points corresponding to qualitative changes in the characteristics of the microwave radiation of the underlying surface. Point 1 (JD_1) corresponds to the temperature at which saline water begins to freeze (changes in its state of aggregation as a result of ice formation). Point 2 (JD_2) corresponds to an ice thickness equal to the skin layer. A further increase in ice thickness does not lead to a noticeable change in T_b, which depends on the ice temperature and the presence of snow patches on the ice surface during thaws [31]. Points 3 (JD_3) and 4 (JD_4) correspond to the beginning and end of the melting of saline ice. In accordance with this, a specific feature becomes the existence of four phases of the state of the surface of a reservoir with different radio-emitting characteristics, depending on the temperature and salinity of water, the thickness, temperature and salinity of ice: ($JD_1 - JD_2$) – open water; ($JD_2 - JD_3$) – formation of ice cover with ice thickness $d \le L$ (L – ice skin layer); ($JD_3 - JD_4$) – established ice cover with thickness $d \ge L$; ($JD_4 - JD_1$) – melting of ice cover.

For the southern part of the Caspian Sea, T_b(JD) (see Fig. 2b) has the appearance characteristic of mineral reservoirs that do not freeze throughout the year. In this case, T_b of the water surface depends on the temperature and salinity of water [16, 30], as well as on sea waves and the formation of foam on the sea surface [37].

Figure 2c shows dependences T_b(JD) for Kara-Bogaz-Gol Bay, which is the world's largest mirabilite deposit and is characterized by a high concentration of salts dissolved in water (from 270 to 380‰ depending on the season, the water surface temperature and the level of the Caspian Sea, which contribute to the shallowing of the bay) [4, 5]. As can be seen from the graphs, T_b(JD) and T(JD) are in antiphase (the minimum T_b values correspond to the maximum T values and vice versa). This behavior of T_b(JD) may be associated with the characteristics of the dissolution of salts in water and the characteristics of their precipitation.

Significant hydrological changes are occurring in the drainless bitter Lake Sarykamysh, which has been operating since the 1960s as a water receiver for collector-drainage waters generated in the Khorezm (Uzbekistan) and Dashkhauz (Turkmenistan) regions. Over the past 35 years, Lake Sarykamysh turned from small salt marshes into the largest irrigation and discharge reservoir in the Aral Sea basin. The mineralization of the water in the lake is sodium chloride, salinity reaches 15–20‰. In the last decade, studies of the hydrological state of Lake Sarykamysh, as well as other water bodies of the Aral–Caspian region, have been carried out using space sensing methods [6].

Dependence T_b(JD) for Lake Sarykamysh is shown in Fig. 2d. During the winter periods of 2011/2012, of 2012/2013, and 2013/2014, ice cover formed on the water surface of the lake, which is confirmed by satellite images in the optical range (https://worldview.earthdata.nasa.gov). From the end of 2014 to the present, no ice cover has formed, which may be due to an increase in the mass concentration of soluble salts brought by collector-drainage waters.

The Aral Sea (AS), which has been subjected to catastrophic drying out since the 1960s, has undergone the most noticeable hydrological changes [11, 22, 26–29]. From the analysis of T_b(JD) dependences for the western (see Fig. 2e) and northern (see Fig. 2f) parts of the AS, as well as satellite images in the optical range, it follows that, in the western part of the AS, the ice cover last formed in 2012. The northern part of the AS is characterized by annual formation of ice cover varying in the duration of periods of open water and ice.

One of the largest bitter lakes in the south of Western Siberia and the largest in Altai krai is Lake Kulunda, the area of which during the summer season can change by 25% (depending on the weather conditions and the dryness of the year). Accordingly, with a change in the area of the lake, the salinity of the water also changes [1, 7]. Figure 2g shows T_b(JD) and T(JD) calculated for Lake Kulunda. The dynamics of the temperature of the lake's water surface were determined using *MODIS* data. T values are averaged over the lake area. Since the lake area is smaller than the pixel of the MIRAS radiometer, the lake T_b values were recalculated using formula (1) for a cell formed only by the steppe and a cell formed by Lake Kulunda (35%) and adjacent steppe territories (65%).

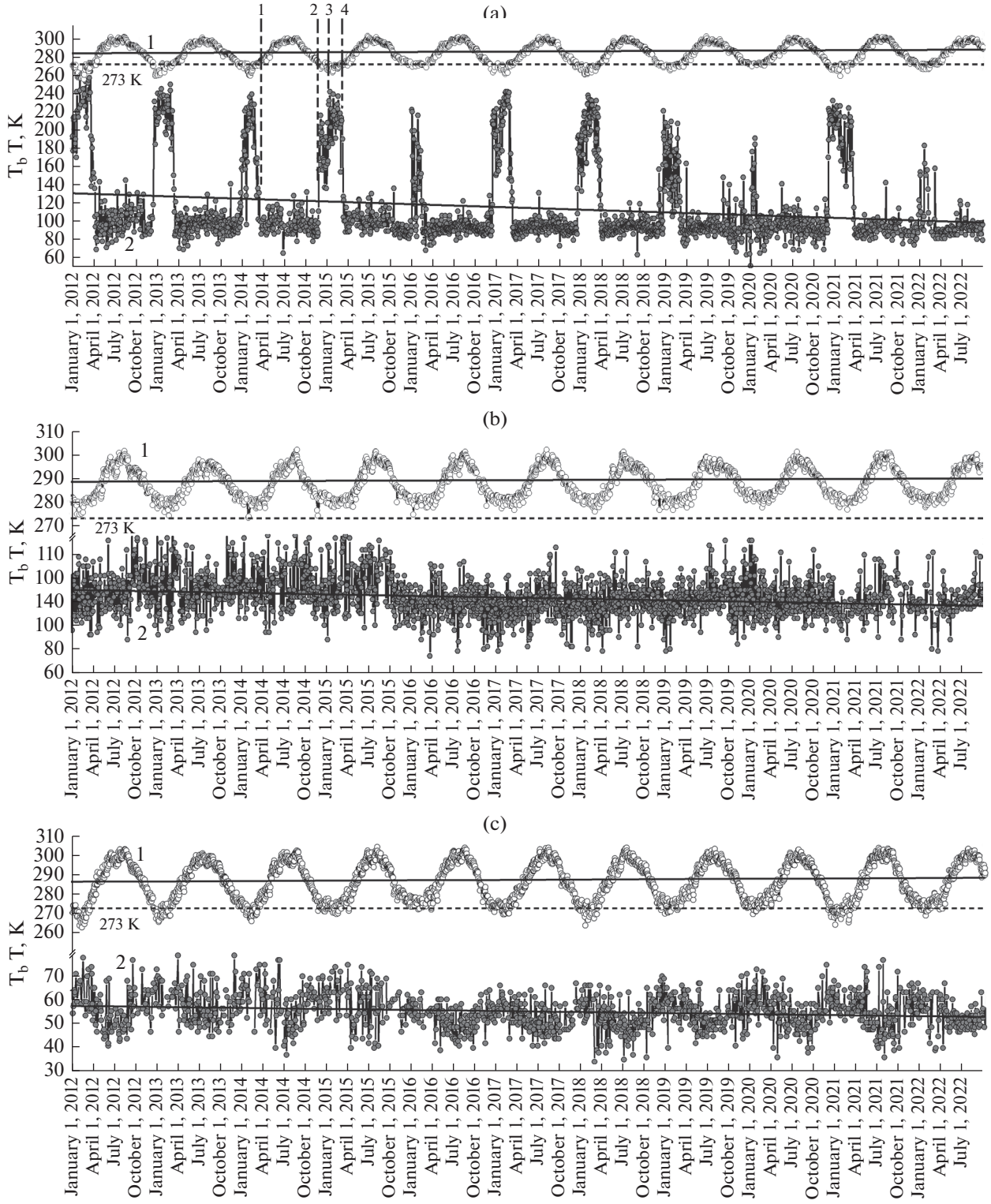

Fig. 2. a–c. Seasonal dynamics of (*1*) thermodynamic and (*2*) radio brightness temperatures measured on horizontal polarization at a sounding angle of 42.5° for the (a) northern and (b) southern parts of the Caspian Sea and (c) Kara-Bogaz-Gol Bay. **d–f.** Seasonal dynamics of (*1*) thermodynamic and (*2*) radio brightness temperatures measured on horizontal polarization at a sounding angle of 42.5° for (c) Kara-Bogaz-Gol Bay, (d) Lake Sarykamysh, and (e) western and (f) northern parts of the Aral Sea. **g, h.** Seasonal dynamics of (*1*) thermodynamic and (*2*) and radio brightness temperatures measured on horizontal polarization at a sounding angle of 42.5° for (g) Lake Kulunda and (h) Lake Ubsu-Nur (explanations in the text).

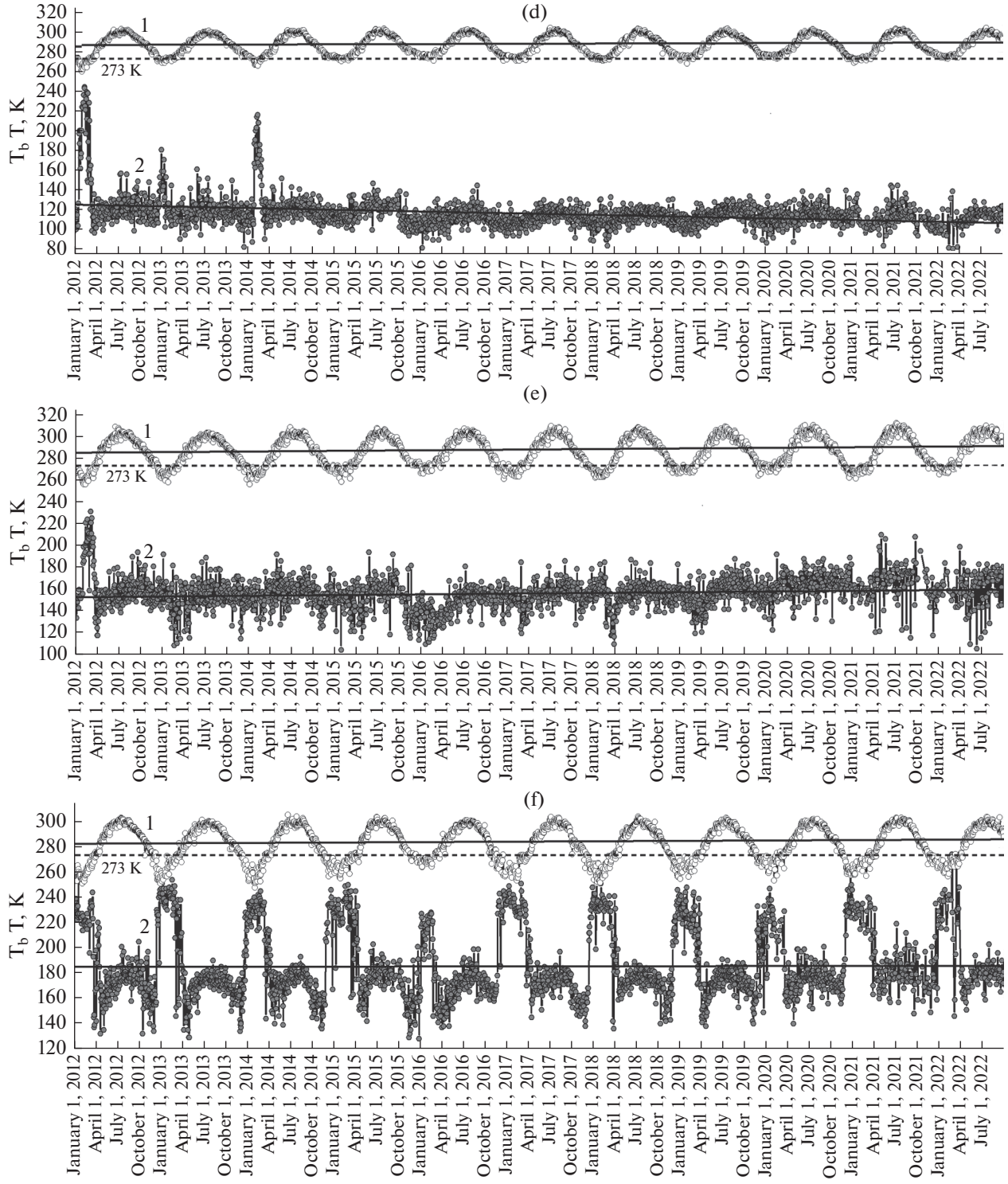

Fig. 2. (Contd.)

Figure 2h shows T_b(JD) and T(JD) dependences for the largest lake in Mongolia, Ubsu-Nur (T data measured at the weather station WMO_ID 44212 (World Meteorological Organization Identifier) (Ulangom: 49°59′ N, 92°05′ E; 939 m), taken from the meteorological site rp5.ru (https://rp5.ru)). The hydrological features of the lake depend largely on variations in salinity and freeze-up conditions [8]. Noteworthy are the annual sharp decreases in T_b, which can be associated both with rainfall in the winter–spring season, and with the earlier opening of rivers and flooding of the lake ice cover with river water. The emergence of a multilayer

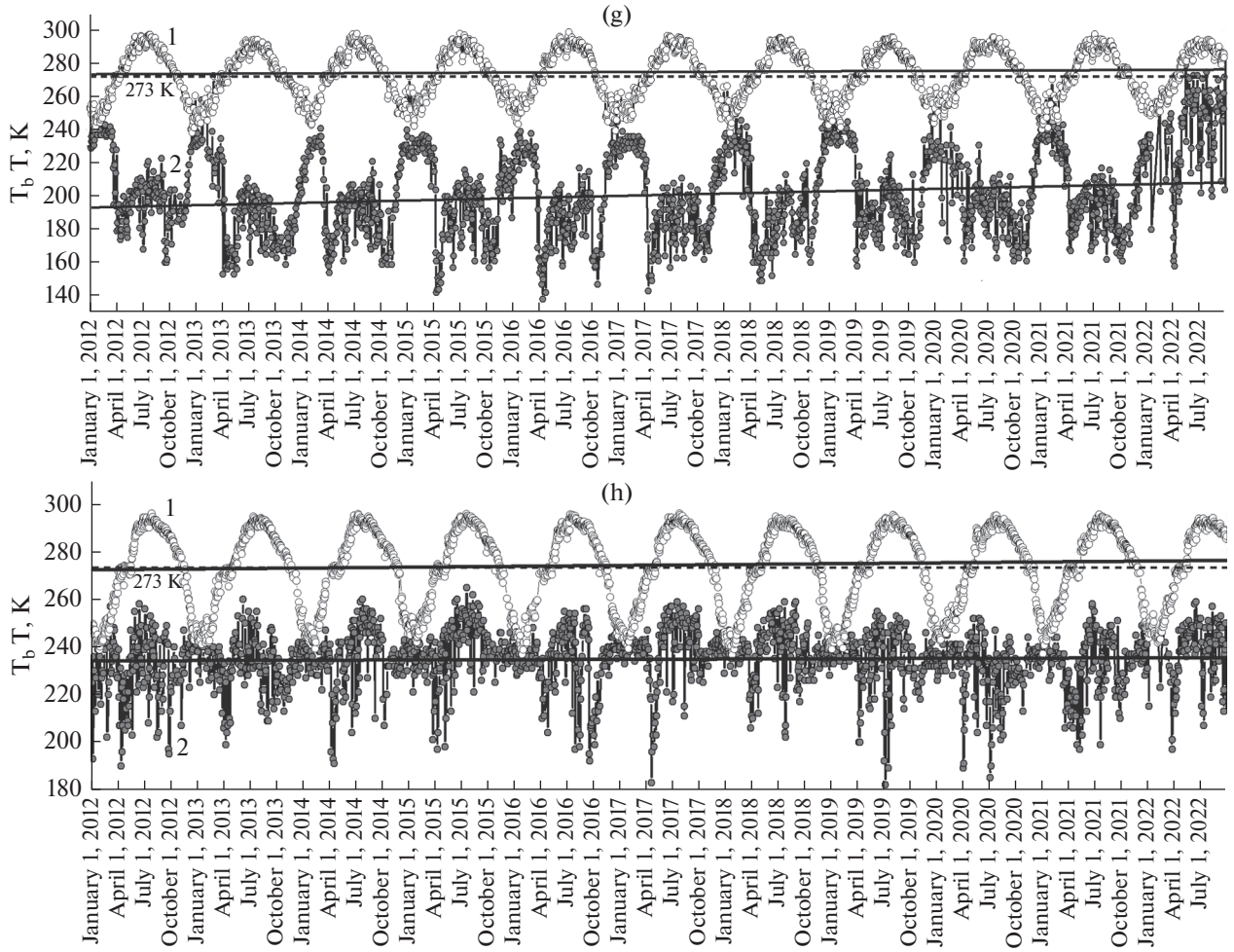

Fig. 2. (Contd.)

structure, which forms in the spring as a result of surface melting of ice and subsequent freezing of melted water, is accompanied by sharp short-term changes in the radio-emitting characteristics of the underlying surface. This allows for early identification of the onset of melting and obtaining additional information about the state of ice cover [9].

Dependences T_b(JD) and T(JD) for the studied lakes shown in Fig. 2 were approximated by straight lines having the following form:

$$T_b = A + B\text{JD}, \quad (2)$$

$$T = C + D\text{JD}, \quad (3)$$

where A, B, C, and D are numerical coefficients given in Table 1.

The difference in coefficients indicates differences in hydrological changes in different regions of Northern Eurasia. From the analysis of satellite data, it follows that T increases for all studied lakes at different rates, which may be due to differences in climatic conditions. At the same time, the T_b value for different mineral lakes behaves differently. The reasons for the decrease in T_b for lakes located in the southern part of Northern Eurasia may be a reduction in the duration of the cold period (due to increased temperature), fluctuations in the water level in lakes, and increased evaporation and, accordingly, an increase in water salinity, leading to a decrease in the emissivity of the water surface. For mineral lakes located at higher latitudes, an increase in T_b may be associated with seasonal processes of melting snow cover in the spring and a decrease in water salinity, as well as shallowing of lakes at the end of the summer season, the formation of stable ice cover.

CONCLUSIONS

A joint analysis of satellite data from *SMOS* and *MODIS* made it possible to identify noticeable seasonal variations in the microwave radiation of mineral lakes. It has been shown that the patterns of long-term seasonal dynamics of radio brightness temperature of mineral lakes in Northern Eurasia differ significantly.

Table 1. Numerical coefficients A, B, C, D in formulas (2), (3)

Object	Seasonal ice cover	A	$B \times 10^{-4}$	σ	C	$D \times 10^{-4}$	σ
1	+	20276	–82.0	0.040	–2214	10.2	0.010
2	–	4319	–17.2	0.050	–585	3.6	
3		3038	–12.1	0.030	–1013	5.3	
4		11748	–47.3	0.090	–1348	6.6	
5		–4211	17.8	0.010	–3466	15	
6	+	–413	2.4	0.100	–1872	8.8	
7		–9269	38.5	0.030	–1479	7.1	0.030
8		–625	3.5	0.001	–2198	10.1	0.005

σ is standard deviation.

For mineral lakes with a seasonal ice cover forming on the water surface, four time intervals have been identified in dependence T_b(JD), in each of which the radio brightness characteristics of the water surface depend on the rate of ice formation or melting, temperature changes and water salinity.

FUNDING

The research was supported by the Russian Science Foundation, grant no. 22-17-20041, https://rscf.ru/project/22-17-20041/.

CONFLICT OF INTEREST

The authors of this work declare that they have no conflicts of interest.

REFERENCES

1. Galakhov, V.P., Conditions for the formation of surface runoff in the Kulunda lake basin, *Izv. Altaisk. Gos. Univ.,* 2003, no. 3 (29), pp. 71–78.
2. Ginzburg, A.I., Kostianoi, A.G., and Sheremet, N.A., Seasonal and interannual variability of the surface temperature in the Caspian Sea, *Oceanology,* 2004, vol. 44, no. 5, pp. 605–618.
3. Ginzburg, A.I., Kostianoy, A.G., Serykh, I.V., and Lebedev, S.A., Climatic changes in hydrometeorological parameters of the Caspian Sea (1980–2020), *Sovremennye problemy distantsionnogo zondirovaniya Zemli iz kosmosa,* 2021, vol. 18, no. 5, pp. 277–291. https://doi.org/10.21046/2070-7401-2021-18-5-277-291
4. Ginzburg, A.I., Kostyanoy, A.G., and Sheremet, N.A., On the dynamics of waters in the Kara-Bogaz-Gol Bay (satellite information), *Sovremennye problemy distantsionnogo zondirovaniya Zemli iz kosmosa,* 2022, vol. 19, no. 4, pp. 265–279. https://doi.org/10.21046/2070-7401-2022-19-4-265-279
5. Karpychev, Yu.A., Variations in the sedimentation in Kara Bogaz Gol bay related to sea level fluctuations during the novocaspian time, *Oceanology,* 2007, vol. 47, no. 6, pp. 857–864. . https://doi.org/10.1134/S0001437007060100
6. Kostyanoy, A.G., Lebedev, S.A., Lavrova, O.Yu., Soloviev, D.M., and Solov'ev, D.M., Satellite monitoring of the waters of Turkmenistan, *9-ya Vserossiiskaya otkrytaya konferentsiya "Sovremennye problemy distantsionnogo zondirovaniya Zemli iz kosmosa"* (9th All-Russia Open Conf. "Current Problems in Remote Sensing of the Earth from Space"), Nov. 14–18, 2011, Moscow, 2011, p. 271. http://conf.rse.geosmis.ru/thesisshow.aspx?page=30&thesis=2898.
7. Lebedeva (Verba), M.P., Lopukhina, O.V., and Kalinina, N.V., Specificity of the chemical and mineralogical composition of salts in solonchak playas and lakes of the Kulunda steppe, *Pochvovedenie,* 2008, no. 4, pp. 467–480.
8. Stepanenko, V.M., Repina, I.A., Ganbat, G., and Davaa, G., Numerical simulation of ice cover of saline lakes, *Izvestiya, Atmospheric and Oceanic Physics,* 2019, vol. 55, no. 1, pp. 129–138. https://doi.org/10.1134/S0001433819010092
9. Anderson, M.R., Crane, R.G., and Barry, R.G., Characteristics of arctic ocean ice determined from SMMR data for 1979: Case studies in the seasonal sea ice zone, *Advances in Space Research,* 1985, vol. 5, no. 6, pp. 257–261. https://doi.org/10.1016/0273-1177(85)90329-1
10. Gorji, T., Sertel, E., and Tanik, A., Monitoring soil salinity via remote sensing technology under data scarce conditions: A case study from Turkey, *Ecological Indicators,* 2017, vol. 74, pp. 384–391. . https://doi.org/10.1016/j.ecolind.2016.11.043
11. Guo, H., Bao, A., Liu, T., Jiapaer, G., Ndayisaba, F., Jiang, L., Kurban, A., and De Maeyer, P., Spatial and temporal characteristics of droughts in Central Asia during 1966–2015, *Sci. Total Environ.,* 2018, vol. 624, pp. 1523–1538. https://doi.org/10.1016/j.scitotenv.2017.12.120
12. Gutierrez, A., Castro, R., and Vieira, P., SMOS L1 Processor L1c Data Processing Model, SO-DS-DME-

L1OP-0009, 2014, no. 2.14. https://earth.esa.int/documents/10174/1854456/SMOS_L1c-Data-Processing-Models.

13. Kamilli, K.A., Ofner, J., Krause, T., Sattler, T., Schmitt-Kopplin, P., Eitenberger, E., Friedbacher, G., Lendl, B., Lohninger, H., Schöler, H.F., and Held, A., How salt lakes affect atmospheric new particle formation: A case study in Western Australia, *Sci. Total Environ.,* 2016, vol. 573, pp. 985–995. https://doi.org/10.1016/j.scitotenv.2016.08.058
14. Moore J. N., Recent desiccation of Western Great Basin saline lakes: Lessons from Lake Abert, Oregon, USA, *Sci. Total Environ.,* 2016, vol. 554–555, pp. 142–154. https://doi.org/10.1016/j.scitotenv.2016.02.161
15. Njoku, E.G. and Kong, J.A., Theory for passive microwave remote sensing of near surface soil moisture, *J. Geophys. Res.,* 1977, vol. 82, pp. 3108–3118. https://doi.org/10.1029/JB082i020p03108
16. Olmedo, E., Martínez, J., Umbert, M., Hoareau, N., Portabella, M., Ballabrera-Poy, J., and Turiel, A., Improving time and space resolution of SMOS salinity maps using multifractal fusion, Remote Sensing of Environment, 2016, vol. 180, pp. 246–263. https://doi.org/10.1016/j.rse.2016.02.038
17. Panciera, R., Walker, J.P., Kalma, J., and Kim, E., A proposed extension to the soil moisture and ocean salinity level 2 algorithm for mixed forest and moderate vegetation pixels, *Remote Sens. Environ.,* 2011, vol. 115, no. 12, pp. 3343–3354. https://doi.org/10.1016/j.rse.2011.07.017
18. Poursanidis, D. and Chrysoulakis, N., Remote Sensing, natural hazards and the contribution of ESA Sentinels missions, *Remote Sensing Applications: Society and Environment,* 2017, vol. 6, pp. 25–38. https://doi.org/10.1016/j.rsase.2017.02.001
19. Romanov, A.N., Khvostov, I.V., and Sukovatova, A.Yu., Seasonal variations of microwave radiation of saline soils in the Kulunda stepped on evidence derived from SMOS, *Progress in Electromagnetics Research Symp.—Spring (PIERS),* 2017, pp. 3025–3031. https://doi.org/10.1109/PIERS.2017.8262274
20. Roy, S.K., Rowlandson, T.L., Berg, A.A., Champagne, C., and Adams, J.R., Impact of sub-pixel heterogeneity on modelled brightness temperature for an agricultural region, *Int. J. Appl. Earth Observ. Geoinf.,* 2016, vol. 45, pp. 212–220. https://doi.org/10.1016/j.jag.2015.10.003
21. Rüdiger, C., Walker, J.P., Kerr, Y., Kim, E.J., Hacker, J.M., Gurney, R.J., Barrett, D., and Marshall, J.L., Toward vicarious calibration of microwave remote-sensing satellites in arid environments, *IEEE Trans. Geosci. Remote Sens.,* 2014, vol. 52, no. 3, pp. 1749–1760. https://doi.org/10.1109/TGRS.2013.2254121
22. Russell, A., Ghalaieny, M., Gazdiyeva, B., Zhumabayeva, S., Kurmanbayeva, A., Akhmetov, K.K., Mukanov, Y., McCann, M., Ali, M., Tucker, A., Vitolo, C., and Althonayan, A., A spatial survey of environmental indicators for Kazakhstan: An examination of current conditions and future needs, *Int. J. Environ. Res.,* 2018, vol. 12, no. 5, pp. 735–748. https://doi.org/10.1007/s41742-018-0134-7
23. Sahr, K., White, D., and Kimerling, A.J., Geodesic discrete global grid system, *Cartography and Geographic Information Science,* 2003, vol. 30, no. 2, pp. 121–134. https://doi.org/10.1559/152304003100011090
24. Shao, Y., Wang, L., Wang, G., Chai, X., Gao, Z., Zhang, T., Gong, H., and Liu, C., Lake Lop Nur evolution analysis based on radar polarimetric decomposition technology, *IEEE Geoscience and Remote Sensing Symp.,* 2014, pp. 2731–2733. https://doi.org/10.1109/IGARSS.2014.6947040
25. Sharkov, E.A., *Passive Microwave Remote Sensing of the Earth: Physical Foundations,* Berlin: Springer PRAXIS, 2003.
26. Sharma, A., Huang, H.P., Zavialov, P., and Khan, V., Impact of desiccation of Aral Sea on the regional climate of Central Asia using WRF model, *Pure Appl. Geophys.,* 2018, vol. 175, no. 1, pp. 465–478. https://doi.org/10.1007/s00024-017-1675-y
27. Shen, H., Abuduwaili, J., and Ma, L., Remote sensing-based land surface change identification and prediction in the Aral Sea bed, Central Asia, *Int. J. Environ. Sci. Technol.,* 2019, vol. 16, no. 4, pp. 2031–2046. https://doi.org/10.1007/s13762-018-1801-0
28. Singh A., Behrangi A., Fisher J. B., Reager J. T., On the desiccation of the south Aral Sea observed from spaceborne missions, *Remote Sens.,* 2018, vol. 10, no. 5, p. 793. https://doi.org/10.3390/rs10050793
29. Sun, F. and Ma, R., Hydrologic changes of Aral Sea: A reveal by the combination of radar altimeter data and optical images, *Annals of GIS,* 2019, vol. 25, no. 3, pp. 247–261. https://doi.org/10.1080/19475683.2019.1626909
30. Talone, M., Sabia, R., Camps, A., Vall-llossera, M., Gabarró, C., and Font, J., Sea surface salinity retrievals from HUT-2D L-band radiometric measurements, *Remote Sens. Environ.,* 2010, vol. 114, no. 8, pp. 1756–1764. https://doi.org/10.1016/j.rse.2010.03.006
31. Tikhonov, V.V., Repina, I.A., Raev, M.D., Sharkov, E.A., Ivanov, V.V., Boyarskii, D.A., Alexeeva, T.A., and Komarova, N.Yu., A physical algorithm to measure sea ice concentration from passive microwave remote sensing data, *Adv. Space Res.,* 2015, vol. 56, no. 8,pp. 1578–1589. https://doi.org/10.1016/j.asr.2015.07.009
32. Ulaby, F.T., Moor, R.K., and Fung, A.K., *Microwave Remote Sensing: Active and Passive,* in 3 vol., Addison-Wesley Publ. Company, 1986.
33. Waiser, M.J., and Robarts, R.D., Saline inland waters, in *Encyclopedia of Inland Waters,* Elsevier, 2009, vol. 2, pp. 634–644.
34. Wang, J., Guo, N., and Ma, C., The dynamic variation characteristics of Gahai Lake area based on EOS-MODIS data, *IEEE Int. Geoscience and Remote Sensing*

Symp., 2012, pp. 768–771.
https://doi.org/10.1109/IGARSS.2012.6351451

35. Wigneron, J.-P., Schwank, M., Baeza, E.L., Kerr, Y., Novello, N., Millan, C., Moisy, C., Richaume, P., Mialon, A., Al Bitar, A., Cabot, F., Lawrence, H., Guyon, D., Calvet, J.-C., Grant, J.P., Casal, T., de Rosnay, P., Saleh, K., Mahmoodi, A., Delwart, S., and Mecklenburg, S., First evaluation of the simultaneous SMOS and ELBARA-II observations in the Mediterranean region, *Remote Sens. Environ.,* 2012, vol. 124, pp. 26–37.
https://doi.org/10.1016/j.rse.2012.04.014
36. Yan, L. and Zheng, M., Influence of climate change on saline lakes of the Tibet Plateau, 1973–2010, *Geomorphology,* 2015, vol. 246, pp. 68–78.
https://doi.org/10.1016/j.geomorph.2015.06.006
37. Yin, X., Boutin, J., Martin, N., and Spurgeon, P., Optimization of L-Band Sea surface emissivity models deduced from SMOS data, *IEEE Trans. Geoscience and Remote Sensing,* 2012, vol. 50, no. 5, pp. 1414–1426.
https://doi.org/10.1109/TGRS.2012.2184547

Translated by S. Avodkova

SPELL: OK